JTTEE5 19:1244–1254
DOI: 10.1007/s11666-010-9532-x
1059-9630/$19.00 © ASM International

Microstructural Development and Deposition Behavior of Titanium Powder Particles in Warm Spraying Process: From Single Splat to Coating

KeeHyun Kim, Seiji Kuroda, and Makoto Watanabe

(Submitted March 23, 2010; in revised form July 8, 2010)

Warm spraying has been developed by NIMS, in which powder particles are accelerated and simultaneously heated, and deposited onto a suitable substrate in thermally softened solid state. In this study, commercially available titanium powder was sprayed onto steel substrate by the spraying process. Microstructural developments and deposition behaviors from a deposited single particle to a thick coating layer were observed by high resolution electron microscopes. A single titanium particle sprayed onto the substrate was severely deformed and grain-refined mainly along the interfacial boundary of particle/substrate by the impact of the sprayed particle. A successive impact by another particle further deformed the previously deposited particle and induced additional grain refinement of the remaining part. In a thick coating layer, the severe deformation and grain refinement were also observed. The results have demonstrated the complex deposition behavior of sprayed particles in the warm spraying using thermally softened metallic powder particles.

Keywords bonding mechanism, dynamic recrystallization, grain refinement, transmission electron microscopy, warm spraying

1. Introduction

Kinetic spraying processes such as cold spray (Ref 1-8), kinetic metallization (Ref 9, 10), high velocity air fuel (HVAF) process (Ref 11-13), and warm spray (Ref 14-16) use mainly the kinetic energy of sprayed powder particles in solid state to make a coating. When the velocity of sprayed particles exceeds a critical value, bonding of particle and substrate can be formed by the so-called shear instability in heavily deformed region, which is resulted from the local and abnormal heating and softening of the material (Ref 3-5, 17). When the velocity is increased excessively, however, erosion of the sprayed powder can occur, and consequently, much of the sprayed particles cannot remain bonded on the substrate (Ref 4, 14). Therefore, to avoid such excessive increase of the velocity, and at the same time, to increase the necessary deformation for the bonding, one should increase the temperature of in-flight powder (Ref 16, 18). For that, in warm spraying, powder is accelerated and simultaneously heated by a controlled high-temperature supersonic gas flow without any preheating of process gas or powder, and finally, it is bonded to substrate (Ref 14-16), while in other spraying processes such as cold spraying, the preheating of process gas or powder before spraying is needed (Ref 8, 19, 20).

Mechanical properties of coated materials depend fundamentally on their microstructures and nature of bonding. In the spraying processes using the warm powder, the thermal and kinetic energy of sprayed particles transferred from the propellant gas flow can change the microstructure of sprayed particles and a resultant coating layer. Several studies have shown the microstructural features of deposited single particles (Ref 16, 21-23) or thick coated layers (Ref 6, 7, 24-26) with discussions about possible bonding mechanisms. In this study, the microstructural developments as well as the deposition behaviors from a deposited single particle to a thick coating layer were demonstrated and observed by high resolution electron microscopes. Especially, since the interface of particle and substrate is very narrow and the internal microstructure of particles is deformed in nanometer scale, transmission electron microscopy (TEM) was used to resolve the microstructures. The internal microstructure of splat was previously studied by TEM (Ref 16, 18, 21-23). However, in those studies, the splat size was less than about 5 μm because it is a limitation to avoid bending of thin membranes in the focused ion beam (FIB) lift-out

This article is an invited paper selected from presentations at the 4th Asian Thermal Spray Conference (ATSC 2009) and has been expanded from the original presentation. ATSC 2009 was held at Nanyang Hotel, Xi'an Jiaotong University, Xi'an, China, October 22-24, 2009, and was chaired by Chang-Jiu Li.

KeeHyun Kim, Seiji Kuroda, and **Makoto Watanabe**, Hybrid Materials Center, National Institute for Materials Science (NIMS), Tsukuba, Japan. Contact e-mail: kim.keehyun@nims.go.jp.

process. Therefore, it remained necessary to study much bigger splat than 5 μm in order to generalize the observed microstructural developments and deposition behaviors of the small-sized particles. In this study, thin electron-transparent samples for TEM observations were made at jetted-out, bonded, and center-bottom regions separately, out of three different splats with the diameter of about 30 μm. Furthermore, since actual coating layer is formed by successive impacts of sprayed particles, i.e., after one layer of sprayed particles is deposited on substrate successive titanium particles impact onto the previously deposited titanium particles and consequently effects of the successive impacts on the previously deposited particles were also studied. Finally, the microstructures in a thick coating were investigated.

2. Experimental

2.1 Feedstock Material, Spraying Process, and Conditions

Single titanium powder particles were deposited on steel substrate by the so-called wipe test at a low powder feeding rate of 4 g/min and a high spray gun transverse speed of 1500 mm/s by the warm spraying process using commercially available titanium powder (TILOP-45 μm, Sumitomo Titanium Corp., Tokyo, Japan). The powder measured by the laser scattering method (Microtrac 9320-X100, USA) and confirmed by electron microscopy has a Gaussian powder size distribution from 1 to 45 μm with the volume average of 28 μm (Ref 16). In the process, the combustion gas flow made by kerosene and oxygen is mixed with inert nitrogen gas to lower its temperature. The temperature-controlled gas flow can accelerate and simultaneously heat the feedstock powder. Then, the sprayed powder particles can be deposited and bonded to a substrate. In this study, nitrogen flow rate was 1.5 m^3/min, which is an optimized spraying condition to induce unmolten in-flight titanium particles (Ref 15, 16) and relatively high bonding strength (Ref 27). The detailed spraying parameters used in this study were summarized in Table 1. In the process, the calculated and measured velocity and temperature were about 700 m/s and 1100 K, respectively, for titanium powder with 30-μm diameter (Ref 15, 23). To investigate the effect of successive impacts on the previously deposited particle, double splats which were impacted vertically or laterally were made by higher powder feeding rate during a single scan of a spraying gun. Then, a thick coating layer with about 400-μm thickness was made with the spraying parameters shown in Table 1.

Table 1 List of spray parameters

Parameter	Splat	Coating
Fuel flow rate, dm^3/min	0.30	0.30
Oxygen flow rate, dm^3/min	623	623
Nitrogen flow rate, dm^3/min	1500	1500
Barrel length, mm	200	200
Spraying distance, mm	180	180
Powder feed gas	Nitrogen	Nitrogen
Substrate temperature, °C	25	25
Spray gun traverse velocity, mm/s	1500	700
Powder feed rate, g/min	4	27

2.2 Microstructure Observation and TEM Sample Preparation

As-deposited splats were observed by a field emission scanning electron microscope (FE-SEM, JEOL JSM-6500). The cross-sectional thin sections of splats were exquisitely prepared at the central region of each splat by ion milling (Hitachi FB-2100) using a focused gallium ion beam (FIB). Then, the inside microstructure of each splat was observed by a FE-TEM (JEOL JEM-2100F) with scanning TEM (STEM) mode and a normal TEM (JEOL JEM-2000FX) each operating at 200 kV. TEM specimens were made at the desired location in deposited splats or a coating layer by the FIB lift-out technique (Ref 16, 23).

2.3 Numerical Simulation

In order to understand deformation behaviors during successive impact and to correlate with TEM observation, the finite element simulations of two particles were carried out by using a commercial code (ABAQUS/explicit version 6.5). Figure 1 shows the model configuration used in this study. Two-dimensional plain strain model was adopted by referring to the multiple particle impact simulation carried by Bae et al. (Ref 17). Two particles with diameter D (30 μm) were impacting on substrate by turns. The second particle would be impacted on the previous deposited particle at 30 ns later in vertical impacting, or 39 ns in lateral impacting after the first particle was impacted on substrate. The center position of the second particle was initially $1.7D$ away from the substrate surface in the vertical, and the offset distance between the first and second particles was D in the lateral. Three-Node linear plane strain elements were used. The initial element size was about $D/50$ of the particle size near contact surfaces and adaptive remeshing was applied to avoid calculation errors due to huge distortion of the elements near the contact surface. Johnson-Cook plastic deformation model was applied to express high strain rate plastic hardening of the materials (Ref 28-30). It takes into account strain hardening and thermal softening effects, and strain rate dependence (Ref 3, 5, 17, 30, 31).

$$\sigma = [A + B\varepsilon^n][1 + C \ln \varepsilon^*][1 - T^{*m}]$$

where σ is the equivalent flow stress, A is the yield stress, B is the strain hardening coefficient, ε is the equivalent plastic strain, n is a power exponent of the strain hardening, C is the dimensionless strain rate coefficient, ε* is the normalized strain rate, $T^* = (T - T_{ref})/(T_m - T_{ref})$ where T_m is the melting point, and T_{ref} is room temperature, and m is a power exponent of the thermal softening. The material properties of titanium and medium carbon steel (JIS S45C) used in the analyses have been shown in Table 2 (Ref 28-32). Note that most of parameters were

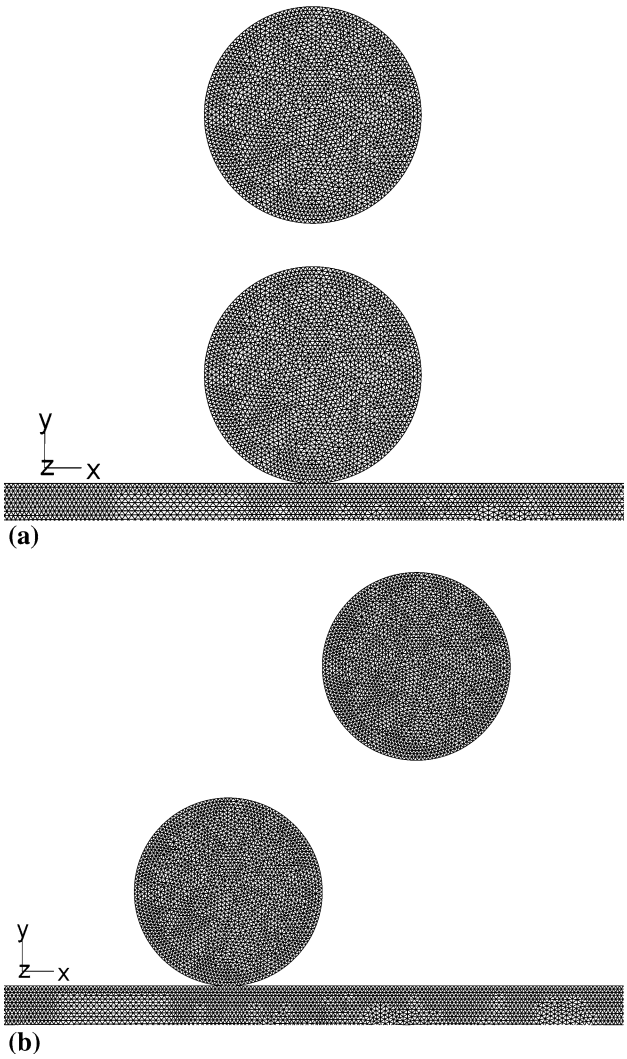

Fig. 1 Model configurations used for numerical simulations of vertical impacting (a) and lateral impacting (b)

Table 2 Parameters in Johnson-Cook deformation model for room temperature case

Parameter	Ti	S45C
Yield stress (A), MPa	480	175
Strength coefficient (B), MPa	1352	380
Strain rate coefficient (C)	0.04	0.06
Strain hardening exponent (n)	0.27	0.32
Melting temperature, K	1941	1809
Reference temperature, K	293	293
Reference strain rate, 1/s	1	1
Thermal softening exponent (m)	1	0.55

set as a function of temperature (Ref 31, 32). Calculations were done under an assumption of adiabatic process. Initial velocity and temperature of both particles were assumed as 700 m/s and 1100 K, respectively. The substrate temperature was set to room temperature.

3. Results and Discussion

3.1 Single Titanium Powder Particle Impacted on Steel Substrate

Figure 2 shows the SEM images of as-received titanium powder and deposited particles on a steel substrate. The powder has nearly spherical shape before spraying. Titanium particles with the estimated velocity of about 700 m/s and temperature of about 1100 K were impacted on the substrate (Fig. 2b). At the spraying condition, splashed or disk-shaped splats were not observed, which can be observed in molten splats (Ref 16). Therefore, nearly all the particles were deposited in solid state because they did not reach the melting point during the spraying as simulated based on the gas dynamics modeling (Ref 15). Since the temperature of sprayed particles at the moment of impact onto the substrate is high enough to induce their thermal softening, the particles were well deformed and adhered to the substrate regardless of the original powder size.

Figure 3 shows a schematic diagram of an in-flight particle onto substrate and observed microstructures. A top view (Fig. 3b) and a side view image (Fig. 3c), respectively, of a single splat show that the deposited splat was heavily deformed in solid state because a splat formed by a molten particle becomes more extensively and uniformly flattened (Ref 16, 33) instead of the curved edge as observed in these figures. Figure 3(d) shows a cross-sectional image of a splat prepared by the FIB milling method. It clearly shows the heavy deformation and the occurrence of jetting-out of the deposited particle, which are indispensible to make the bonding of sprayed particles and substrate (Ref 31). The jetting-out phenomenon indicates that the material underwent a kinetic to thermal energy transition leading to softening of the sprayed particle. Furthermore, the softening combined with high strain and strain rates can induce the severe deformation of the splat and mix or remove the oxide(s) existing on the surfaces of splat and substrate (Ref 18, 22, 31, 34). Consequently, intimate bonding between a particle and a substrate can be formed.

The inside microstructure of splats at the jetted-out, the bonded, and the center-bottom regions of a splat, each prepared from three different splats with the diameter of about 30 μm, was observed using TEM. Figure 4 shows TEM images of each region of the big splats. In the bonded region (Fig. 4b), the particle and the substrate were intimately bonded without any voids or gaps. Moreover, a thin amorphous layer was also observed in the region as observed in small-size splats (Ref 23). In Fig. 4(c), the impact of the particle onto substrate could induce easily the jetting-out phenomenon because sprayed particles in the warm spraying process are severely deformed and thermally softened (Ref 22, 23). In the center-bottom region (Fig. 4d), a thin void was observed, which might be induced by the accumulated strain energy or thermal stress during impact (Ref 17, 31). Furthermore, since commercially pure titanium and titanium alloys form easily the so-called adiabatic shear bands upon high strain and high strain-rate loading due to the tendency of

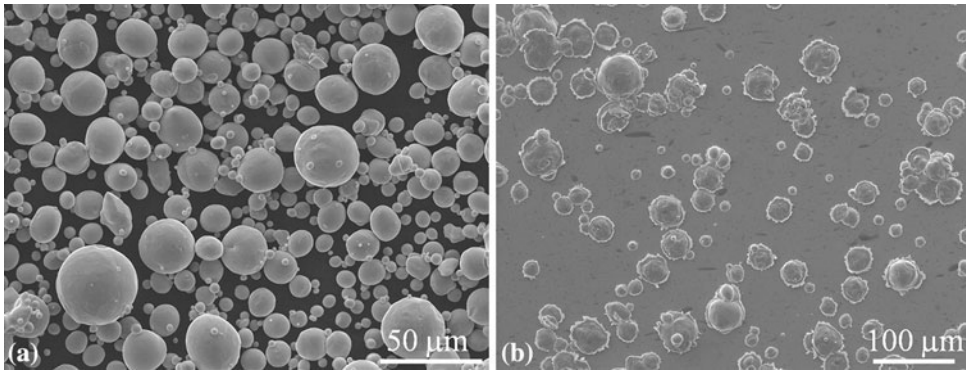

Fig. 2 SEM image of as-received titanium powder particles (a) and deposited particles (b)

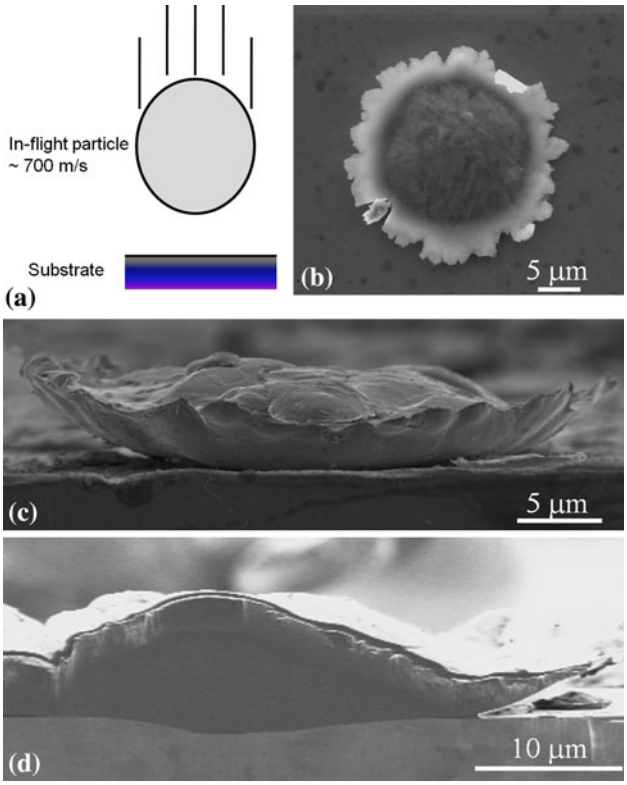

Fig. 3 Schematic diagram of an in-flight particle impacting onto substrate (a), SEM top-view image (b) and side view (c), and cross-sectional secondary ion image of a deposited particle (d)

localized deformation (Ref 21, 35), microstructural alternations such as the formation of extremely fine grains with nano-size were formed along the interfacial boundary of particle and substrate by dynamic recrystallization as shown in Fig. 4(d). These observed microstructural development and deposition behavior of relatively big-sized particles are similar to those of small-sized splats in the previous studies by the authors (Ref 16, 21, 22). Therefore, in the next section, small-sized splats were used to investigate the effects of successive impacts on the microstructure and deposition behavior of sprayed particles because they are appropriate to show a whole image of deposited particles as well as to make thin membranes for TEM observations without bending of the sample (see and compare the splat size in Fig. 3 with that in Fig. 5 or 7).

3.2 Successive Impact of Another Particle onto a Deposited Particle

After one layer of sprayed particles is deposited onto substrate, successive sprayed particles impact onto the previously deposited particles. The successive impacts can be classified into two cases: one is the vertical impact of another successive particle onto the previously deposited particle, and the other is the lateral impact (Ref 18).

3.2.1 Vertical Impact. Figure 5 shows the effect of a successive vertical impact on the previously deposited particle. In Fig. 5(a), another in-flight particle (denoted as P-B) with the velocity of about 700 m/s and temperature of about 1100 K is approaching on the deposited particle (P-A) which is the same one as that described in section 3.1. A SEM image (Fig. 5b) of the impacted two splats shows that the second P-B particle was deposited on the center of the first P-A particle incidentally. A TEM sample was made at the center region of the vertically impacted two splats. Figure 5(c) shows the vertical cross-sectional TEM image. It clearly shows that the center-upper region of the previously deposited P-A particle was severely deformed due to the successive impact of the subsequently deposited P-B particle. Furthermore, a bright field STEM image of Fig. 5(d) near the center region of two splats shows that dynamic recrystallization of the P-A particle occurred within the whole particle, while in the P-B particle, the recrystallization occurred only along the interface as indicated by the selected area diffraction patterns. Compared with the result of single splat deposited on the substrate (Fig. 4), the center-upper region of the previously deposited particle (marked with D in Fig. 5d) could be severely deformed and experience dynamic deformation behavior by the successive impact. In the jetted-out region (Fig. 5e), both splats were grain-refined by the recrystallization. It should be noted, however, that as a void was observed in the center-bottom region of the single deposited particle (Fig. 4d); a void was

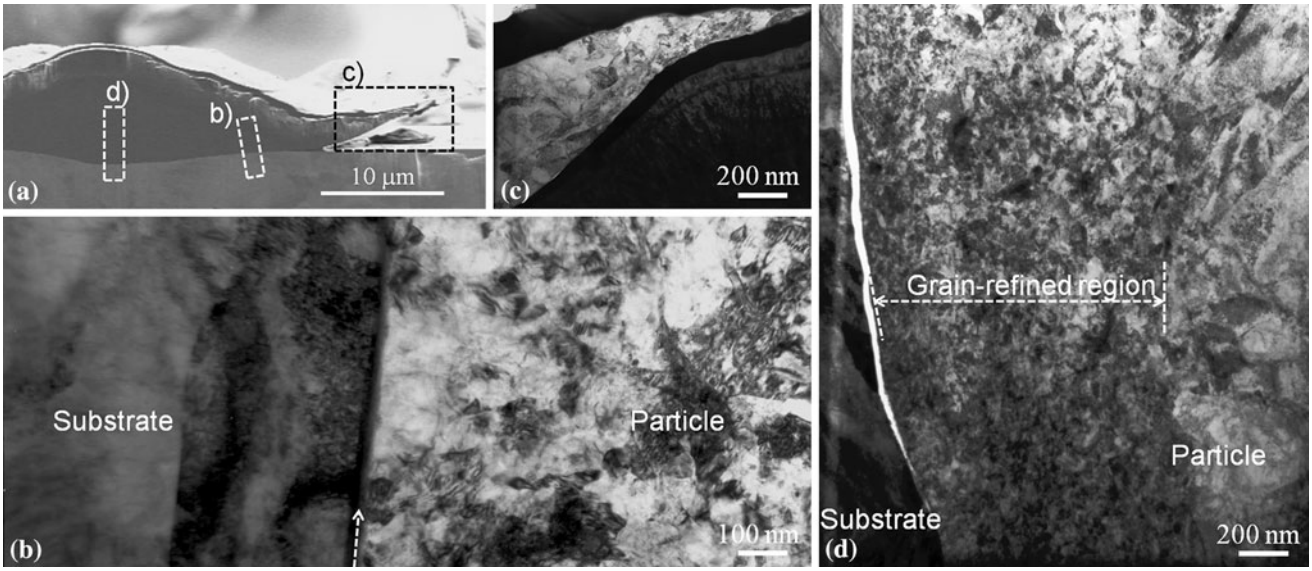

Fig. 4 TEM sampling position (a) and TEM images in the bonded (b), the jetted-out (c), and the center-bottom region (d). In (b), the arrow indicates a boundary layer in the interface of substrate/particle. Note that the grain-refined region occurred within the limited region along the boundary of particle and substrate and a void formed between them

also observed between the previously (P-A) and the subsequently (P-B) deposited particles.

The strain and stress evolutions at the vertically impacted two particles were estimated by Finite Element Modeling (FEM) as shown in Fig. 6. The P-B particle was impacted onto the P-A particle at 30 ns later after the P-A particle had impacted on substrate. As shown in Fig. 5, the subsequently impacted P-B particle could deform severely the previously deposited P-A particle. In the modeling of single impact of a sprayed particle, as soon as a sprayed particle impacted onto the substrate, extremely high compressive stress were developed but the stress became tensile after about 100 ns (Ref 31). If this tensile stress at the center-bottom region of single splat exceeded the bonding strength between the particle and the substrate, then it might be able to cause rebounding or detaching the deposited particle from the substrate (Ref 31). However, in the modeling of successive impact, if the subsequently deposited particle (the P-B particle in this study) can impact onto the previously deposited particle (the P-A particle) before generating the tensile stress, it would compress the center-bottom region of the previously deposited particle and prevent the rebounding or detaching. In addition, within such short period of 100 ns, the previously deposited particle could be still hot and softened enough to deform more. Therefore, the void formed between the previously deposited particle and the substrate or between the previously and subsequently deposited particles might be minimized or annihilated by the consecutive impacts of sprayed particles with strong kinetic energy, see the interface of the P-A particle and the substrate in Fig. 5(d) and Ref 34.

3.2.2 Lateral Impact. Figure 7 shows the effect of another successive impact of sprayed particles. A sprayed particle (P-D in Fig. 7) impacted laterally to a previously deposited particle (P-C). A top view SEM image of the two splats shows that the jetted-out region of subsequently impacted particle (P-D) met laterally the previously deposited particle (P-C) incidentally. A TEM specimen was exquisitely made near the impacted region by the FIB lift-out technique. A STEM image in Fig. 7(c) shows that the jetted-out region of the P-C particle was heavily distorted by the lateral impact of the P-D particle, while that of the P-D particle was preserved. It means that strong impact by a subsequently deposited particle can easily deform a previously deposited particle. In Fig. 7(c), it should be noted that the left part of the P-D particle was milled away and the electron transparent region was re-thinned by the FIB lift-out technique (see the detailed re-thinning process in our Ref 36). Therefore, the STEM bright field image of splats in Fig. 7 is brighter than that of splats which was not re-thinned in Fig. 5.

Such lateral impact was also simulated by the FEM as shown in Fig. 8, where another particle (P-D) impacted laterally onto a previously deposited particle (P-C) at a distance of the diameter (D, 30 μm) of the particles at 39 ns after the P-C particle had impacted on the substrate. The impact of the P-D particle severely deformed the jetted-out region of the P-C particle. Figure 8(b) shows evolutions of the equivalent plastic strain (PEEQ), which is a parameter to express strain in triaxial stress, at three points in the P-D particle along the boundary with the P-C particle. The evolution shows that the strain in the jetted-out region (C region in Fig. 8a) increased dramatically, which is a mark of the occurrence of shear instability. Strong shear stress inducing the abnormal increase of strain and the instability could easily deform the previously deposited P-C particle. The severe plastic work can

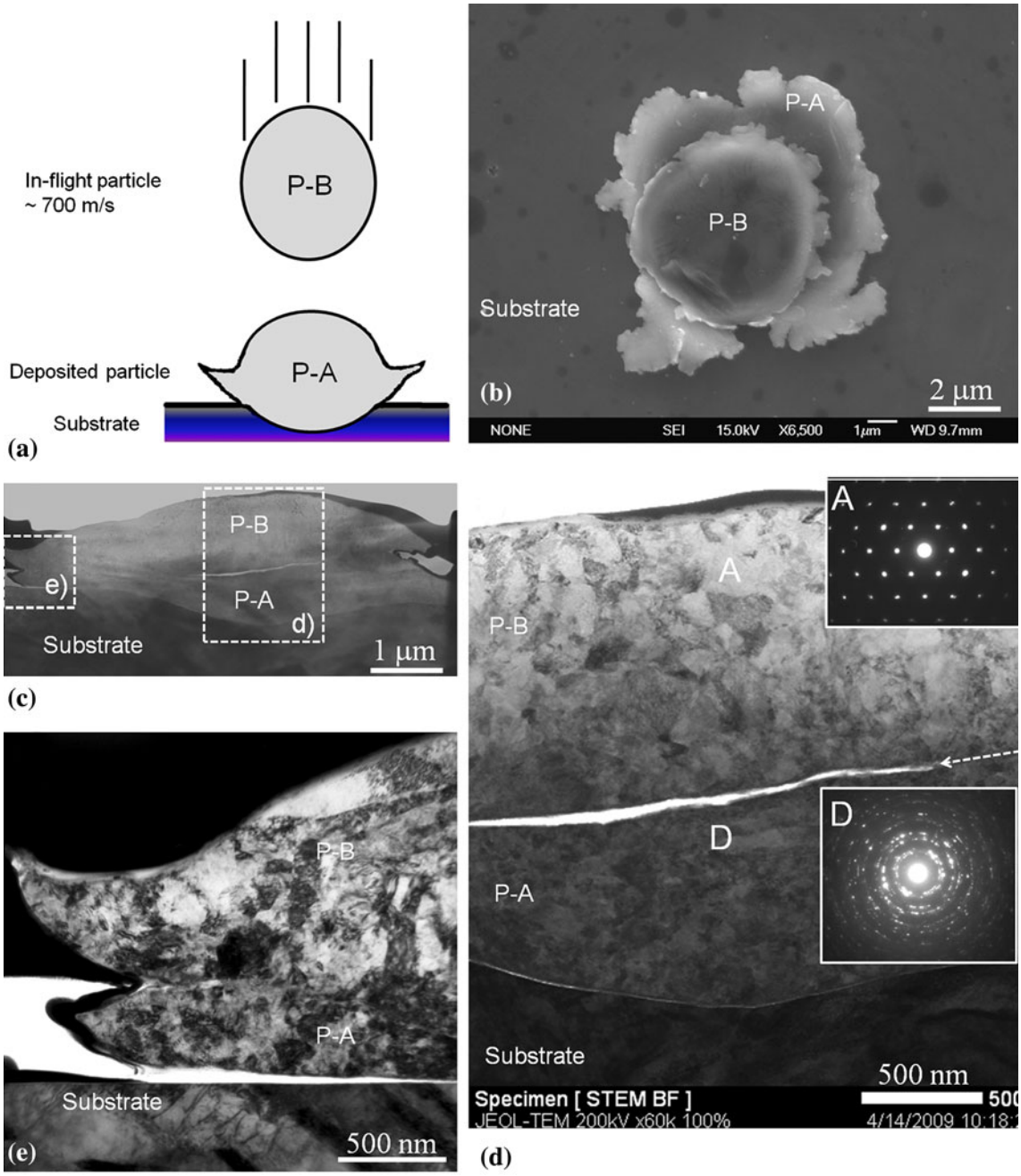

Fig. 5 Schematic diagram of an in-flight particle impacting onto a deposited particle (a), SEM image of another titanium particle (denoted as P-B) deposited on the previously deposited particle (P-A) (b), vertical cross-sectional normal TEM image in low magnification (c), and magnified images (d and e) at the marked regions in panel (c). In (d), the diffraction patterns were acquired, respectively, at the selected areas of A and D, and the arrow indicates a void formed between P-A and P-B particles

also heat the jetted-out and the deformed regions (Ref 3, 4). In the FEM, the jetted-out region in the P-C particle, which had undergone large deformation, could remain hot at the onset of the impact of the P-D particle because it takes about 100 ns or more until the region is completely cooled down (Ref 3, 4, 37). Therefore, the region of the P-C particle could be severely deformed by the impact of the P-D particle as shown in Fig. 7 and 8. It means that the impact by a subsequent particle can deform extremely the previously deposited particle which has not been cooled down.

Figure 8(c) shows stress evolutions at the center-bottom region (marked with D in Fig. 8a) of the previously deposited P-C particle. Compared with that of the vertical impact of Fig. 6(b), the lateral impact could induce much stronger tensile stress. Therefore, the lateral impact might

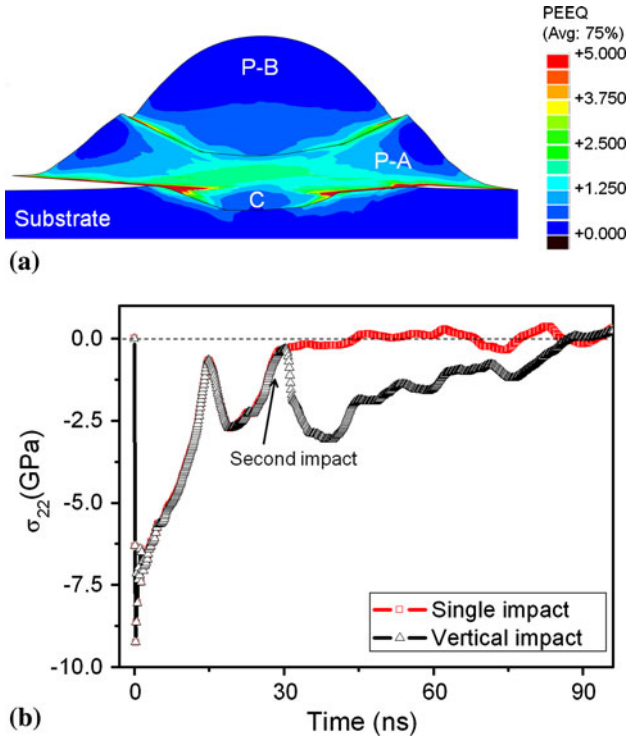

Fig. 6 Contours of the equivalent plastic strain (PEEQ) of vertically impacted two splats (a) and stress development (b) at the center-bottom region (marked with C in (a)) of the previously deposited P-A particle. Note that the particle shapes were not symmetric in (a) because there were some numerical deviations in every increment during 1000 step

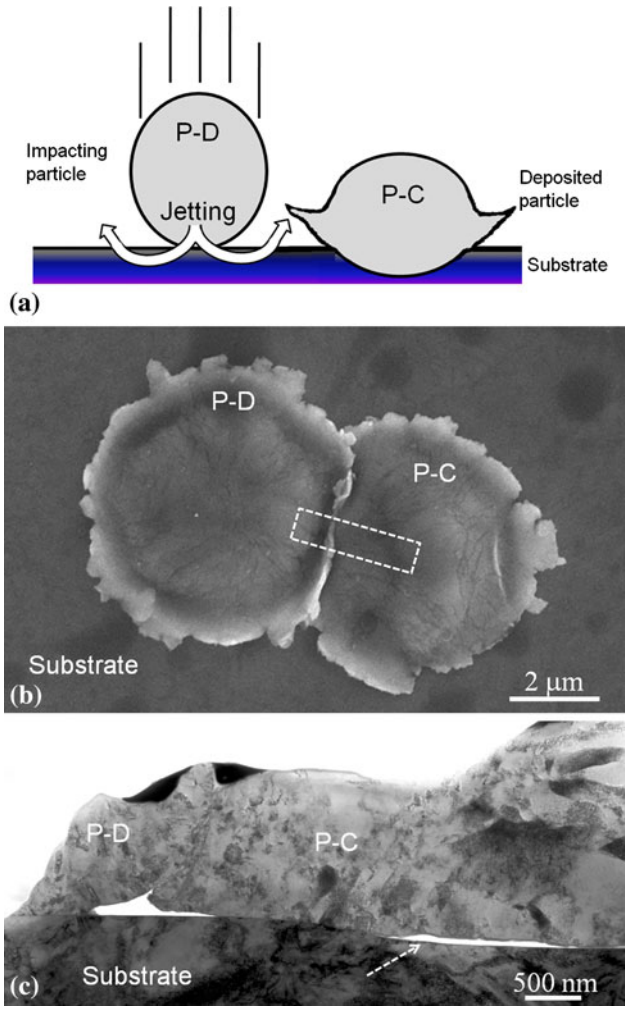

Fig. 7 Schematic diagram of an in-flight particle (P-D) impacting laterally onto a deposited particle (P-C) (a), corresponding SEM image of laterally impacted two particles (b), and vertical cross sectional TEM image (c). TEM sample was made at the marked region in (b) by FIB lift-out technique. The left part of particle P-D was milled away during the sampling process. An arrow in (c) indicates a void formed at the center-bottom of the previously deposited particle

not be able to minimize or annihilate the void form in the center-bottom region of deposited particles. On the contrary, the lateral impact may enlarge the void.

3.3 Thick Coating Formation

In the formation of a thick coating layer, many particles are deposited onto the previously deposited particles. Therefore, whichever substrate we may use, the target surface onto which sprayed particles impact will be changed to the previously deposited particles themselves after single layer of sprayed particles is deposited as shown in Fig. 9(a). During the deposition, the previously deposited particles were heavily deformed at various impacting modes by many particles as well as by the vertical and the lateral impacts. By the multiple impacts, finally, a thick coating layer was formed as shown in Fig. 9(b). However, in a coating layer, the multiple impacts can induce many diverse microstructures such as fine grains, grain growth, and twinning, which could be observed according to the sampling position for TEM observation (Ref 38). Therefore, in this study, only the interfacial region of titanium coating layer and steel substrate was mainly observed to investigate the bonding formation between the coating layer and the substrate and the microstructure.

Figure 10 shows the interfacial region of sprayed particles and substrate. The coating layer and the substrate were intimately bonded as shown in Fig. 10(a). The high kinetic energy of sprayed particles and the tamping effect by successively impacted particles could induce the intimate bonding. Furthermore, the titanium coating was composed of many nanostructured grains induced by the dynamic recrystallization (Fig. 10b). Compared to the result of single splat, the nanograin size of about 5 nm in this study was smaller than that of about 10-50 nm in single splat (Ref 21, 22). The finer grain size in the coating might result from re-grain refinement of each splat induced by many successively impacted particles because the refined grains in single splats could be continuously deformed and heated by the multiple impacts in a coating process. Energy filtered TEM (EF-TEM) images of titanium and iron (Fig. 10c, d) clearly show that there was no intermetallic compound of iron and titanium because, in the spraying processes, the time staying in the temperature

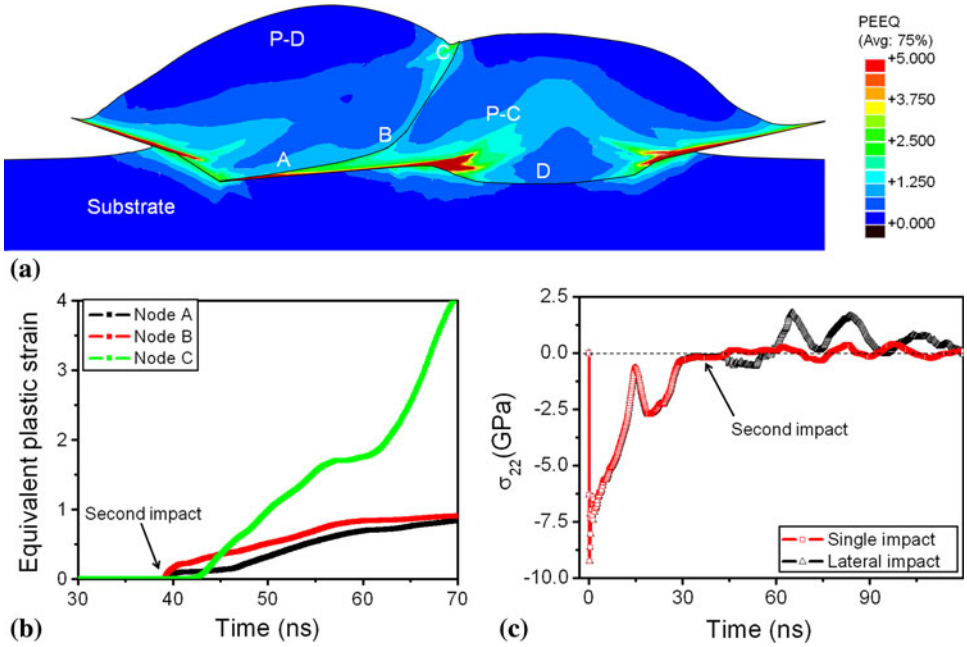

Fig. 8 Contours of the equivalent plastic strain (PEEQ) of laterally impacted two splats (a), equivalent plastic strain (b) at the different node positions in (a), and stress development (c) at the center-bottom region (marked with D in (a)) of the previously deposited P-A particle. An arrow indicates that the second impact by the subsequently deposited P-D particle occurred at the moment

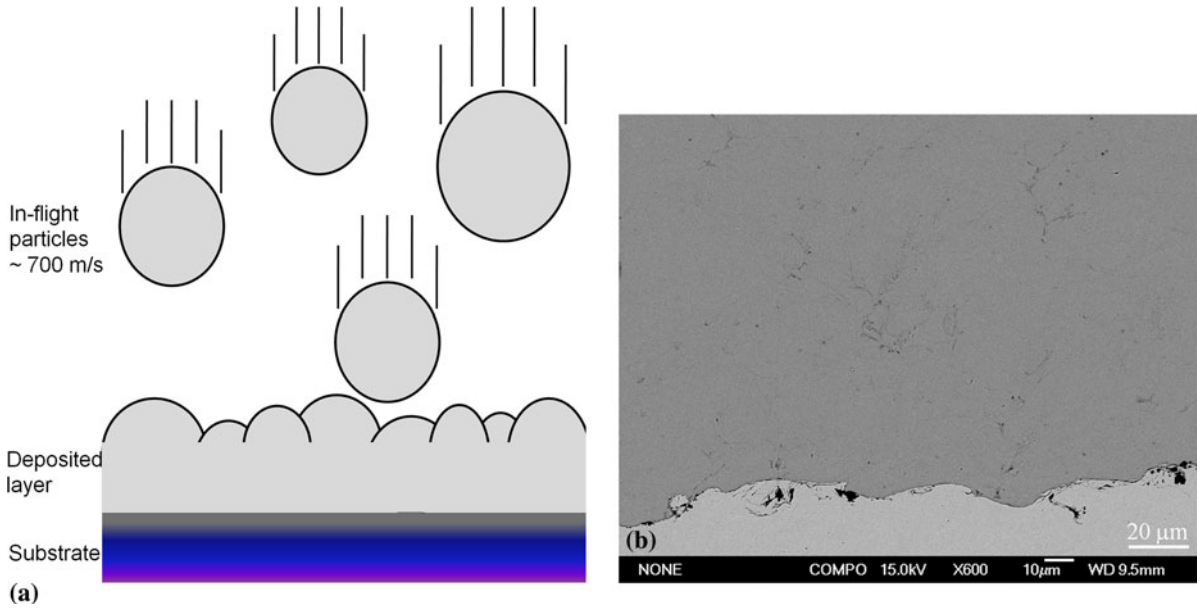

Fig. 9 Schematic diagram of in-flight particles onto deposited layer (a) and SEM image of thickly coated layer (b). Note that the substrate was alumina-blasted before the spraying

range sufficiently high for the diffusion of titanium and/or iron, is too short. By comparison, the oxygen signal for the energy filtered mapping was very low.

Finally, it should be noted that even though a thin amorphous layer including oxygen was observed in the interface of single splat and substrate (Fig. 4b and Ref 23), it was not observed in the interface between thick coating layer and substrate as shown in Fig. 10. The amorphous layer might be crystallized, or the oxygen in the layer might be dissolved into the titanium bulk because of a high solubility of oxygen near 15 mass% (Ref 39) during the spraying process. However, as mentioned previously, the time staying at high temperature is too short to induce the crystallization or the dissolution in the process. Therefore, there is another possibility that the amorphous layer might have

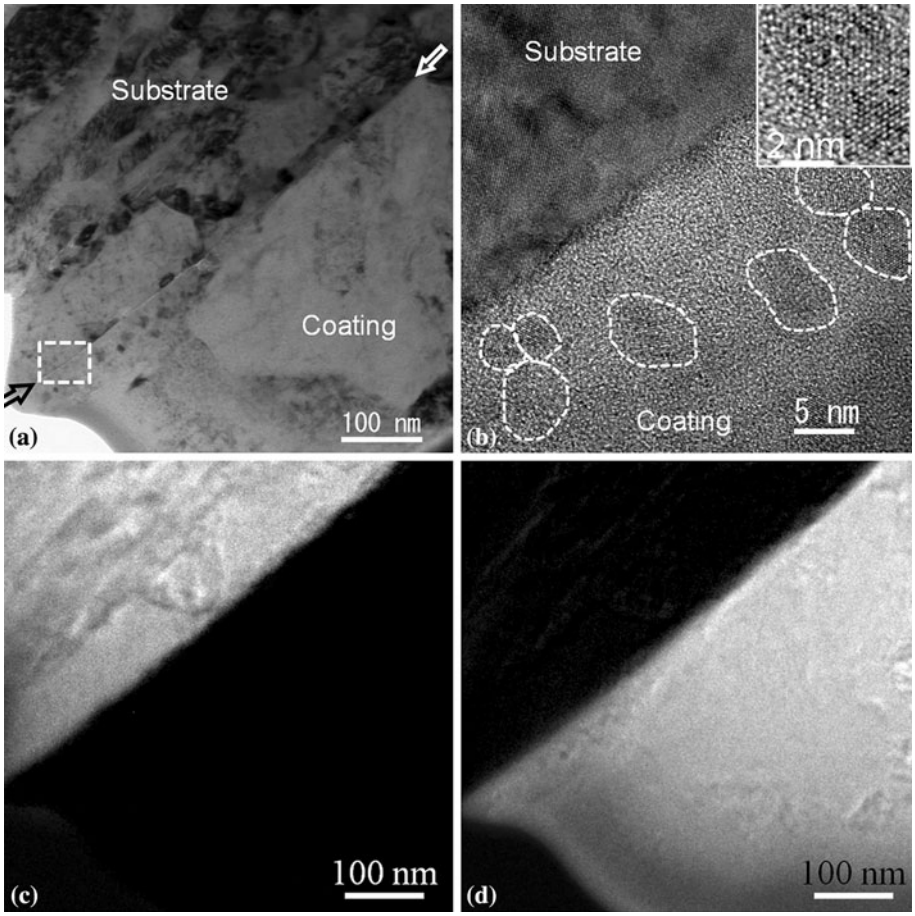

Fig. 10 TEM image near the interface of titanium coating layer and substrate (a), high resolution image (b) at the marked region of (a), and the energy-filtered images of titanium (c) and iron (d). The arrows in (a) indicate the interface of coating/substrate. In (b), very fine grains were indicated, and a grain in high resolution was shown in the inset

been formed by the partial remainder of thin oxide(s) covered with the surface of sprayed particles and/or substrate before impact (Ref 18). Consequently, according to the sampling position of the interface of particle/substrate for TEM observations, the amorphous oxide layer that remained could be observed in some regions, e.g., in the interface as shown in Fig. 4(b) or Ref 23, or no intermediate layer could be observed in some regions, e.g. in the interface in Fig. 10 or Ref 34. If the amorphous layer is completely removed, then the sprayed particle and substrate can make direct metallic bonding (Ref 34). However, even though the layer is not removed, if it is thin and simultaneously exposed to high temperature and pressure, the amorphous layer with high cohesive energy (Ref 18) can also induce the bonding of particle and substrate.

3.4 Remaining Questions About Comparison of Experimental Observation with Simulation

In this section, the general features indentified by TEM observations of small-sized particles (about 5 μm) such as the grain-refined region, the center-bottom void, and the jetting-out phenomenon were compared with the FEM numerical simulation results of big-sized particles (30 μm). Assadi et al. suggested that if the value of $x^2/D_{th}t$ is equal or above 1, in which x represents an element size, D_{th} is thermal diffusivity and t is the process time, then an adiabatic model can be adopted in the simulation (Ref 3). In the warm-spraying process, the value is about 100 (Ref 30). Moreover, the process has negligible time to dissipate the heat induced by impacts of sprayed particles. Consequently, the impact-induced deformation process in this study can be assumed to be adiabatic (Ref 3). In the model, as long as the ratios among the mesh, particle, and substrate sizes are kept constant, the calculation results such as the deformation and temperature distributions are the same in different particle sizes because the adiabatic model does not have the factor affected by the surface area of a particle such as thermal conduction. Yokoyama et al., however, suggested that thermal conduction model should be considered because the heat generated by the impact of sprayed particles can influence the maximum temperature and equivalent plastic strain of both a sprayed particle and substrate (Ref 30). However, in the warm spraying, thermal conduction from the highly deformed interfacial region of particle/substrate to the less deformed inside region in a particle or to substrate during

the impact may not affect largely on the deformation behavior and microstructure of the particle because the whole region of a single sprayed particle is already heated to above $0.5T_m$ before impact and consequently the particle is already thermally softened and possesses enough driving force for the deformation (Ref 34). Moreover, as observed by TEM, the general features of small-sized particles were similar to those of big-sized particles. Therefore, it is considered reasonable to compare the general features (not any specific values such as temperature, strain, and stress) of the TEM result of small-sized particles with the FEM result based on the adiabatic model of big-sized particles in this study.

Finally, the voids that were observed in the center-bottom region of sprayed particles by TEM could not be simulated in the numerical simulation used in this study because modeling of the deposition behavior including bonding criterion is much more complicated. Thus, the precise simulation and interpretation of multiple impacts still remains as a matter for further investigation.

4. Summary

Different samples from a single titanium splat, successively impacted splats, and a thick titanium coating were made by the warm spraying process to investigate the microstructural development and deposition behavior. A single titanium splat was severely deformed, jetted-out by the adiabatic shear instability, and bonded to steel substrate. Furthermore, grain refinement of splat along the interface of particle/substrate was resulted from dynamic recrystallization. Successive impact of another particle had a strong effect on the microstructure of previously deposited particles. The center-upper region of the previously deposited particle, which was not grain-refined before the successive impact, was also grain-refined by the impact. Interestingly, the subsequently impacted particle was only grain-refined along the interface of particle/particle as the grain refinement of single particle occurred along the interface of particle/substrate. The lateral impact of another particle onto the previously deposited particle was also able to severely deform the previously deposited particle. Finally, in a thick coating layer, the grain refinement and the intimate bonding of sprayed particles and substrate were formed by multiple impacts of sprayed particles. The results have demonstrated the complex deposition behavior as well as the microstructural development related to the interaction of sprayed particles in kinetic spraying processes using thermally softened metallic powder particles.

Acknowledgments

The authors would like to thank Dr. K. Mitsuishi of NIMS for his help in the EF-TEM analysis, and Ms. N. Kawano, Mr. M. Komatsu, and Mr. N. Kakeya of NIMS for sample preparations. This research was supported by the Nanotechnology Network program and World Premier International Research Center Initiative on Materials Nanoarchitectonics of MEXT, Japan and KAKENHI 19360335.

References

1. A. Papyrin, V. Kosarev, S. Klinkov, A. Alkhimov, and V. Fomin, *Cold Spray Technology*, Elsevier, Amsterdam, 2007
2. V.K. Champagne, *The Cold Spray Materials Deposition Process*, CRC, New York, 2007
3. H. Assadi, F. Gärtner, T. Stoltenhoff, and H. Kreye, Bonding Mechanism in Cold Gas Spraying, *Acta Mater.*, 2003, **51**(15), p 4379-4394
4. T. Schmidt, F. Gärtner, H. Assadi, and H. Kreye, Development of a Generalized Parameter Window for Cold Spray Deposition, *Acta Mater.*, 2006, **54**(3), p 729-742
5. M. Grujicic, J.R. Saylor, D.E. Beasley, W.S. DeRosset, and D. Helfritch, Computational Analysis of the Interfacial Bonding Between Feed-Powder Particles and the Substrate in the Cold-Gas Dynamic-Spray Process, *Appl. Surf. Sci.*, 2003, **219**(3-4), p 211-227
6. C.J. Li, W.Y. Li, and Y.Y. Wang, Formation of Metastable Phases in Cold-Sprayed Soft Metallic Deposit, *Surf. Coat. Technol.*, 2005, **198**(1-3), p 469-473
7. C. Borchers, F. Gärtner, T. Stoltenhoff, H. Assadi, and H. Kreye, Microstructural and Macroscopic Properties of Cold Sprayed Copper Coatings, *J. Appl. Phys.*, 2003, **93**(12), p 10064-10070
8. G. Bae, S. Kumar, S. Yoon, K. Kang, H. Na, H.J. Kim, and C. Lee, Bonding Features and Associated Mechanisms in Kinetic Sprayed Titanium Coatings, *Acta Mater.*, 2009, **57**(19), p 5654-5666
9. T. Robinson, Coatings: Kinetic Metallization, *2004 MDA Technology Applications Report: Missile Defense Agency*, Advanced Applications Program, 2004, p 36-37
10. R.M. Tapphorn and H. Gabel, The Solid-State Spray Forming of Low-Oxide Titanium Components, *J. Met.*, 1998, **50**(9), p 45-46
11. J.A. Browning, Hypervelocity Impact Fusion—A Technical Note, *J. Therm. Spray Technol.*, 1992, **1**(4), p 289-400
12. W.J. Trompetter, A. Markwitz, and M. Hyland, Role of Oxides in High Velocity Thermal Spray Coatings, *Nucl. Instrum. Methods B*, 2002, **190**, p 518-523
13. Z. Zeng, N. Sakoda, T. Tajiri, and S. Kuroda, Structure and Corrosion Behavior of 316L Stainless Steel Coatings Formed by HVAF Spraying with and without Sealing, *Surf. Coat. Technol.*, 2008, **203**(3-4), p 284-290
14. S. Kuroda, J. Kawakita, M. Watanabe, and H. Katanoda, Warm Spraying—A Novel Coating Process Based on the High-Velocity Impact of Solid Particles, *Sci. Technol. Adv. Mater.*, 2008, **9**(3), p 033002 (17 pp)
15. J. Kawakita, H. Katanoda, M. Watanabe, K. Yokoyama, and S. Kuroda, Warm Spraying: An Improved Spray Process to Deposit Novel Coatings, *Surf. Coat. Technol.*, 2008, **202**(18), p 4369-4373
16. K.H. Kim, M. Watanabe, J. Kawakita, and S. Kuroda, Effects of Temperature of In-Flight Particles on Bonding and Microstructure in Warm Sprayed Titanium Deposits, *J. Therm. Spray Technol.*, 2009, **18**(3), p 392-400
17. G. Bae, Y. Xiong, S. Kumar, K. Kang, and C. Lee, General Aspects of Interface Bonding in Kinetic Sprayed Coatings, *Acta Mater.*, 2008, **56**(19), p 4858-4868
18. K.H. Kim and S. Kuroda, Amorphous Oxide Films Formed by Dynamic Oxidation During Kinetic Spraying of Titanium at High Temperatures and Its Role in the Subsequent Coating Formation, *Scripta Mater.*, 2010, **63**(2), p 215-218
19. X.J. Ning, J.H. Jang, and H.J. Kim, The Effects of Powder Properties on In-Flight Particle Velocity and Deposition Process During Low Pressure Cold Spray Process, *Appl. Surf. Sci.*, 2007, **253**(18), p 7449-7455
20. S. Shin, S. Yoon, Y. Kim, and C. Lee, Effect of Particle Parameters on the Deposition Characteristics of a Hard/soft-Particles Composite in Kinetic Spraying, *Surf. Coat. Technol.*, 2006, **201**(6), p 3457-3461

21. K.H. Kim, M. Watanabe, J. Kawakita, and S. Kuroda, Grain Refinement in a Single Titanium Powder Particle Impacted at High Velocity, *Scripta Mater.*, 2008, **59**(7), p 768-771
22. K.H. Kim, M. Watanabe, and S. Kuroda, Thermal Softening Effect on the Deposition Efficiency and Microstructure of Warm Sprayed Metallic Powder, *Scripta Mater.*, 2009, **60**(8), p 710-713
23. K.H. Kim, M. Watanabe, K. Mitsuishi, K. Iakoubovskii, and S. Kuroda, Impact Bonding and Rebounding between Kinetically Sprayed Titanium Particle and Steel Substrate Revealed by High Resolution Electron Microscopy, *J. Phys. D: Appl. Phys.*, 2009, **42**(6), p 065304 (5 pages)
24. K. Balani, A. Agarwal, S. Seal, and J. Karthikeyan, Transmission Electron Microscopy of Cold Sprayed 1100 Aluminum Coating, *Scripta Mater.*, 2005, **53**(7), p 845-850
25. Y. Xiong, K. Kang, G. Bae, S. Yoon, and C. Lee, Dynamic Amorphization and Recrystallization of Metals in Kinetic Spray Process, *Appl. Phys. Lett.*, 2008, **92**(19), p 194101 (3 pages)
26. A.C. Hall, L.N. Brewer, and T.J. Roemer, Preparation of Aluminum Coatings Containing Homogeneous Nanocrystalline Microstructures Using the Cold Spray Process, *J. Therm. Spray Technol.*, 2008, **17**(3), p 352-359
27. K.H. Kim, M. Watanabe, K. Mitsuishi, J. Kawakita, T. Wu, and S. Kuroda, Microstructure Observation on the Interface between Warm Spray Deposited Titanium Powder and Steel Substrate, *International Thermal Spray Conference and Exposition 2008: Thermal Spray Crossing Borders*, E. Lugscheider, Ed., Jun 2-4, 2008 (Maastricht, The Netherlands), ASM International, 2008, p 1289-1294, CD-ROM
28. G.R. Johnson, Material Characterization for Warhead Computations, *Prog. Astronaut. Aeronaut.*, 1993, **155**, p 165-197
29. S. Seo, O. Min, and H. Yang, Constitutive Equation for Ti-6Al-4V at High Temperatures Measured Using the SHPB Technique, *Int. J. Impact Eng.*, 2005, **31**, p 735-754
30. K. Yokoyama, M. Watanabe, S. Kuroda, Y. Gotoh, T. Schmidt, and F. Gärtner, Simulation of Solid Particle Impact Behavior for Spray Processes, *Mater. Trans.*, 2006, **47**(7), p 1697-1702
31. K.H. Kim, M. Watanabe, and S. Kuroda, Jetting-Out Phenomenon Associated with Bonding of Warm-Sprayed Titanium Particles onto Steel Substrate, *J. Therm. Spray Technol.*, 2009, **18**(4), p 490-499
32. *ASM International Handbook, Vol 8, Mechanical Testing and Evaluation*, Materials Park, OH, 2000
33. T. Chraska and A.H. King, Transmission Electron Microscopy Study of Rapid Solidification of Plasma Sprayed Zirconia. Part I. First Splat Solidification, *Thin Solid Films*, 2001, **397**(1-2), p 30-39
34. K.H. Kim, M. Watanabe, and S. Kuroda, Bonding Mechanisms of Thermally Softened Metallic Powder Particles and Substrates Impacted at High Velocity, *Surf. Coat. Technol.*, 2010, **204**(14), p 2175-2180
35. G.I. Kanel, S.V. Razorenov, E.B. Zaretsky, B. Herrman, and L. Meyer, Thermal ''Softening'' and ''Hardening'' of Titanium and Its Alloy at High Strain Rates of Shock-Wave Deforming, *Phys. Solid State*, 2003, **45**(4), p 656-661
36. K.H. Kim, M. Watanabe, S. Kuroda, and N. Kawano, Observation of Microstructures in Thermal Sprayed Coatings and Single Deposited Splats Using Ion Beam Milling, *International Thermal Spray Conference and Exposition 2010: Thermal Spray: Global Solutions for Future Application*, K. Middeldorf, Ed., May 3-5, 2010 (Singapore), ASM International, 2010, p 1-6, CD-ROM
37. P.C. King, G. Bae, S.H. Zahiri, M. Jahedi, and C. Lee, An Experimental and Finite Element Study of Cold Spray Copper Impact onto Two Aluminum Substrates, *J. Therm. Spray Technol.*, 2010, **19**(3), p 620-634
38. P.C. King and M. Jahedi, Transmission Electron Microscopy of Cold Sprayed Titanium, *International Thermal Spray Conference and Exposition 2010: Thermal Spray: Global Solutions for Future Application*, K. Middeldorf, Ed., May 3-5, 2010 (Singapore), ASM International, 2010, p 1-6, CD-ROM
39. R. Boyer, G. Welsch, and E.W. Collings, *Materials Properties Handbook: Titanium Alloys*, ASM International, Materials Park, 1994